Spectrochimica Acta Part A: Molecular and Biomolecular Spectroscopy 291 (2023) 122319

Contents lists available at ScienceDirect

Spectrochimica Acta Part A:
Molecular and Biomolecular Spectroscopy

journal homepage: www.journals.elsevier.com/spectrochimica-acta-part-a-molecular-and-biomolecular-spectroscopy

Fluorescent boron difluoride curcuminoides as perspective materials for bio-visualization

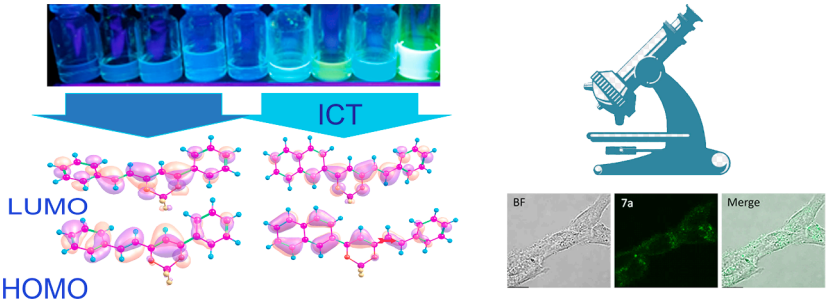
Anatolii G. Mirochnik [a], Zakhar N. Puzyrkov [a,b], Elena V. Fedorenko [a], Irina V. Svistunova [b], Alina A. Markova [c], Anna V. Shibaeva [c], Ivan D. Burtsev [c], Alexey A. Kostyukov [c], Anton E. Egorov [c], Vladimir A. Kuzmin [c]

[a] Institute of Chemistry, Far Eastern Branch, Russian Academy of Sciences, 159, Prosp. 100-letiya Vladivostoka, Vladivostok 690022, Russian Federation
[b] Far Eastern Federal University, 8, Sukhanova Str., Vladivostok 690950, Russian Federation
[c] Emanuel Institute of Biochemical Physics, Russian Academy of Sciences, Moscow, Russian Federation

HIGHLIGHTS

- Curcuminoids of boron difluoride have been synthesized.
- Complexes studied by luminescence spectroscopy and DFT modeling.
- Introduction of π-donor substituents increases luminescence quantum yield.
- Dyes bio-imaging ability and cytotoxicity were investigated.

GRAPHICAL ABSTRACT



ARTICLE INFO

Keywords:
Boron difluoride chelates
Curcuminoids
Luminescence
Bio-visualization
Absorption spectra
TD DFT

ABSTRACT

Curcuminoids of boron difluoride, 1-aryl(hetaryl)-5-phenylpenta-2,4-dien-1-onates of boron difluoride, have been synthesized. A comparative study of the electronic structure, luminescent properties and their potential for applications in bio-imaging has been carried out. The influence of the electronic structure of α-substituents on the luminescence of compounds was studied by the methods of stationary and time-resolved luminescence spectroscopy and DFT modeling. The introduction of π-donor substituents leads to a noticeable bathochromic shift and an increase in the Stokes shift in the luminescence spectra. On going from σ-donor substituents in the phenyl ring to π-donor substituents, the luminescence quantum yield increases from 0.03 to 0.22. The maximum Stokes shift and high quantum yield of luminescence is exhibited by the complex with a stilbene substituent, which has the longest π-system and the maximum efficiency of charge transfer. Dyes are able to penetrate into the cells of the model cell line and accumulate, moreover, accumulation occurs mainly in the cytoplasm of cells. The compounds penetrate into the cells by 12 h of incubation without damaging it's structure and without causing rapid cell death. The submicromolar range of non-toxic concentrations during long-term incubation for a model cell line was determined, which is a characteristic of fluorescent imaging. Due to uniform distribution in the cytoplasm of cells dye with naphtyl substituent is promising for visualization of the cell cytoplasm. This leader compound has the lowest cytotoxicity for cells from the synthesized series of dyes, which makes it promising for further studies as a fluorescent imaging agent.

E-mail address: gev@ich.dvo.ru (E.V. Fedorenko).

https://doi.org/10.1016/j.saa.2023.122319
Received 21 July 2022; Received in revised form 9 December 2022; Accepted 2 January 2023
Available online 4 January 2023
1386-1425/© 2023 Elsevier B.V. All rights reserved.

The leader compound has the lowest cytotoxicity for cells from the synthesized series of dyes, which makes it promising for further studies as a fluorescent imaging agent.

1. Introduction

Organic molecules containing π-conjugated structures comprise promising research objects due to their wide application in the production of smart materials used for the accumulation and storage of information, organic light-emitting diodes (OLEDs), organic light-emitting transistors (OLETs), photo-switching devices, and sensors [1–17].

Unlike most organic compounds [18] β-diketonates of boron difluoride exhibit intense luminescence both in solutions and in crystals [19–21]. Among β-diketonates of boron difluoride, there are compounds luminescing in various ranges from ultraviolet [22] to near infrared range [23]. β-Diketonates of boron difluoride in the crystalline state exhibit size-dependent luminescence [24] as well as reversible thermo- and mechanofluorochromism [25–27].

A systematic study of the luminescent properties of β-diketonates of boron difluoride as potential components of stimuli-response organic materials constitutes an urgent task. The dependence of intermolecular interactions in the solid state on the structure of an individual molecule was discussed and partially found in many works [19–22], however, many factors remain unexplored.

Recently, the attention of researchers was focused on an interesting class of β-diketonates of boron difluoride, curcuminoids, that contain a double bond between the β-diketonate cycle and phenyl substituent, similarly to the complex with curcumin [28] (Fig. 1). Curcuminoids of boron difluoride can be used for bio-visualization, since they are capable to penetrate deep tissues, have a low auto-fluorescence background, and do not cause significant harmful impact to biological specimens [29–34]. These complexes can be used to detect in-vitro insoluble aggregates of amyloid-beta, a pathological sign of the Alzheimer's disease [29], they are HIV-1 and HIV-2 protease inhibitors [30] and capable of binding to fibrillary proteins [31]. A method was developed for the detection of curcumins and their metabolites in brain, liver, and tumor tissues by converting them into boron difluoride curcuminoids followed by analysis using mass-detection chromatography [32].

In the present paper, we studied the luminescence properties of a number of simple boron difluoride curcuminoids: 1-aryl(getaryl)-5-phenylpent-2,4-diene-1-onates of boron difluoride (Fig. 1). These compounds are typical representatives of D-A-D luminophors, in which the difluoroboron fragment acts as an electron acceptor, whereas phenyl rings act as electron donors. These compounds are potentially a good platform for the development of fluorophores for biological or medical applications. The variation of substituents makes it possible to adjust the photophysical and physico-chemical properties of complexes, as well as to control their behavior in biological media.

2. Experimental

2.1. Materials

Benzoylacetone (Alfa Aesar, USA), ethanol, chloroform (EKOS-1, Russia) were used in the present work. Solvent purification was carried out according to the known procedure [35].

Initial boron difluoride β-diketotonates (**1**–**10**) were obtained according to the procedures described earlier: **1** [36], **2**–**6** [37], **7** and **10** [38], **8** [19], **9** [39].

General synthesis method: 0.012 mol of tri(butyl)borate and 0.3 mol of butylamine were added to a solution of 0.010 mol of boron difluoride arenoylacetate and 0.012 mol of benzaldehyde in 30–40 ml of anhydrous ethyl acetate. The reaction mixture was heated with a reverse refrigerator at stirring for 3–4 h. For **2a**, **4a**, **5a**, **7a**, the reaction mixture was held overnight at 5 °C, for the complexes **1a**, **3a**, **6a**, **8a-10a**, the precipitate fell out immediately after cooling to room temperature, and the product was filtered and washed with ethanol. Thereafter, the product recrystallized from acetonitrile.

^{1}H and ^{13}C NMR, IR and mass spectra shown in ESI Figs. 1S–31S.

2,2-Difluoro6-phenyl-4-cinnamoyl-1,3,2-dioxaborine **(1a)** Yellow crystals, yield 31.5 %, melting point 177.8–179.3°s. ^{1}H NMR (400 MHz, $CDCl_3$), δ/ppm: 6.68 (s, 1H), 6.81–6.84 (d, $J = 15.65$ Hz, 1H), 7.41–7.53 (m, 5H), 7.59–7.67 (m, 3H), 8.04–8.08 (m, 3H). ^{13}C NMR (101 MHz, $CDCl_3$), δ/ppm: 97.81, 120.57, 128.84, 129.11, 129.21, 131.79, 131.99, 133.82, 135.14, 147.88, 180.82, 182.52. IR (KBr), υ/cm^{-1}: 3128 (OH_{ass}), 3061, 3032 (C-H_{Ph}), 1637 (C═C), 1597 (C═O), 1541 (C═C), 1377 (δ B-O), 1186, 1151 (δ B-F), 1062 (δ B-O). Anal. calc. for $C_{17}H_{13}BF_2O_2$, %: C, 57.75; H, 3.39 Found, %: C, 57.78; H, 3.42. MS: calcd for $C_{17}H_{13}BF_2O_2$ 298, found $[M-H]^-$ 297.

2,2-Difluoro6-(4′-methylphenyl)-4-cinnamoyl-1,3,2-dioxaborine (**2a**) Yellow crystals, yield 40.5 %, melting point 193.9–194.5 °With. ^{1}H NMR (400 MHz, $CDCl_3$) δ/ppm: 2,44 (3H, CH3), 6,64 (s, 1H), 6,78–6,82 (d, $J = 15.53$ Hz, 1H), 7,29–7,31 (m, 2H), 7,42–7,47 (m, 3H), 7,58–7,60 (m, 2H), 7,96–8,04 (m, 3H). ^{13}C NMR (101 MHz, $CDCl_3$), δ/ppm: 97.52, 120.69, 129.00, 129.11, 129.16, 129.88, 131.78, 133.90, 146.85, 147.18, 180.09, 182.40. IR (KBr), υ/cm^{-1}: 3147 (OH_{ass}), 3058, 3030 (C-H_{Ph}), 1629 (C═C), 1608 (C═O), 1569, 1537 (C═C), 1384 (δ B-O), 1190, 1149, 1126 (δ B-F), 1097, 1076, 1051 (δ B-O). Mass spectrum (ESI-), *m/z* (I, %): 311 [M−H] (100). Anal. calc. for $C_{18}H_{15}BF_2O_2$, %: C, 69.27; H, 4.84. Found, %: C, 69.32; H, 4.80.

2,2-Difluoro6-(4′-ethylphenyl)-4-cinnamoyl-1,3,2-dioxaborine (**3a**). Yellow needle crystals, yield 74.6 %, melting point 176.6–177.9° C. ^{1}H NMR (400 MHz, $CDCl_3$), δ/ppm: 1.28 (3H), 2.74 (2H), 6.64 (s, 1H), 6.81 (d, $J = 15.53$ Hz 1H), 7.34 (d, $J = 8.44$ Hz 2H), 7.41–7.50 (m, 3H), 7.61 (dd, $J = 7.78$, 1.71 Hz, 2H), 7.99–8.05 (m, 3H). ^{13}C NMR (101 MHz, $CDCl_3$), δ/ppm: 97.53, 120.71, 128.70, 129.09, 129.14, 129.17, 129.26, 131.77, 133.93, 147.20, 152.93, 180.09, 182.49. IR (KBr), x/cm^{-1}: 3117 (OH_{ass}), 3065, 3042 (C-H_{Ph}), 1624 (C═C), 1607 (C═O), 1574, 1539 (C═C), 1377 (д B-O), 1182, 1165, 1128 (д B-F), 1059, 1003 (д B-O). Mass spectrum (ESI-), *m/z* (I, %): 325 [M−H] (100). Anal. calc. for $C_{19}H_{17}BF_2O_2$, %: C, 69.97; H, 5.25. Found, %: C, 69.95; H, 5.29.

2,2-Difluoro-6-(3′,4′-dimethylphenyl)-4-cinnamoyl-1,3,2-dioxaborine (**4a**). Dark yellow powder, yield 51.4 %, melting point 219.2–221.1° C. ^{1}H NMR (400 MHz, $CDCl_3$), δ/ppm: 2.30–2.37 (m, 6H), 6.63 (m, 1H), 6.80 (s, 1H), 7.24–7.34 (m, 2H) 7.40–7.47 (m, 3H), 7.60 (dd, $J = 7.58$, 1.83 Hz, 2H), 7.81–7.87 (m, 2H) 8.03 (d, $J = 15.65$ Hz, 1H). ^{13}C NMR (101 MHz, $CDCl_3$), δ/ppm: 97.56, 120.74, 126.71, 127.46, 128.79,

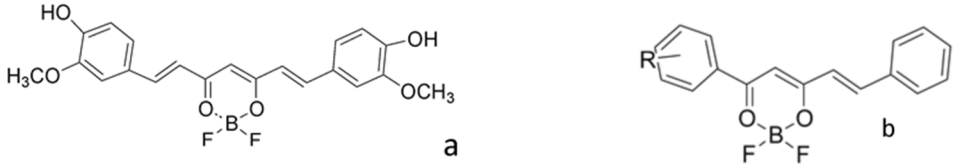


Fig. 1. (a) Boron difluoride complex obtained from natural curcumin, (b) the structure of the studied curcuminoids in general form.

129.06, 129.16, 129.32, 129.93, 130.40, 131.71, 133.95, 137.77, 145.75, 146.98, 179.80, 182.66. IR (KBr), υ/cm^{-1}: 3146 (OH_{ass}), 3059, 3030 (C-H_{Ph}), 1628 (C═C), 1606 (C═O), 1576, 1535 (C═C), 1389, 1364 (δ B-O), 1184, 1169 (δ B-F), 1080, 1055 (δ B-O. Mass spectrum (ESI-), *m/z* (I, %): 325 [M−H] (100). Anal. calc. for $C_{19}H_{17}BF_2O_2$, %: C, 69.97; H, 5.25;. Found, %: C, 70.01; H, 5.28.

2,2-Difluoro-6-(3′,4′- dimethylphenyl)-4-cinnamoyl-1,3,2-dioxaborine (**5**a). Yellow powder, yield 30.7 %, melting point 145–146.5° c. ^{1}H NMR (400 MHz, $CDCl_3$), δ/ppm: 2.38 (s, 3H), 2.58 (s, 3H), 6.42 (s, 1H), 6.80 (d, *J* = 15.65 Hz, 1H), 7.18–7.22 (m, 1H), 7.29 (dd, *J* = 7.70, 1.34 Hz, 1H), 7.42–7.53 (m, 4H), 7.63 (dd, *J* = 7.58, 1.71 Hz, 2H), 8.09 (d, *J* = 15.65 Hz, 1H). ^{13}C NMR (101 MHz, $CDCl_3$), δ/ppm: 101.39, 120.56, 129.15, 129.22, 130.37, 131.91, 132.27, 132.32, 133.87, 134.25, 135.87, 136.74, 147.62, 180.25, 187.16. IR (KBr), υ/cm^{-1}: 3138 (OH_{ass}), 3055, 3024 (C-H_{Ph}), 1626 (C═C), 1529 (C═C), 1385, 1367 (δ B-O), 1186, 1169, 1153 (δ B-F), 1080, 1047 (δ B-O). Mass spectrum (ESI-), *m/z* (I, %): 325 [M−H] (100). Anal. calc. for $C_{19}H_{17}BF_2O_2$, %: C, 69.97; H, 5.25;. Found, %: C, 70.02; H, 5.22.

2,2-Difluoro-6-(4′-methoxylphenyl)-4-cinnamoyl-1,3,2-dioxaborine (**6a**). Yellow crystals, yield 74.5 %, melting point 197.3–198.6° s. ^{1}H NMR (400 MHz, $CDCl_3$) δ/ppm: 3.91 (s, 3H) 6.56 (s, 1H) 6.78 (d, *J* = 15.65 Hz 1H) 6.98 (d, *J* = 9.05 Hz, 2H), 7.39–7.49 (m, 3H), 7.59 (dd, *J* = 7.46, 1.96 Hz, 2H), 8.01–8.07 (m, 3H).^{13}C NMR (101 MHz, $CDCl_3$), δ/ppm: 97.01, 114.60, 120.82, 124.02, 128.97, 129.13, 131.53, 134.05, 146.44, 165.64, 179.04, 181.60. IR (KBr), υ/cm^{-1}: 3130 (OH_{ass}), 3060, 3026 (C-H_{Ph}), 1631 (C═C), 1602 (C═O), 1529 (C═C), 1385, 1367 (δ B-O), 1186, 1169, 1153 (δ B-F), 1080, 1047 (δ B-O). Mass spectrum (ESI-), *m/z* (I, %): 239 [M−$C_6H_4OCH_3$] (100), Anal. calc. for $C_{18}H_{15}BF_2O_3$, %: C, 65.89; H, 4.61. Found, %: C, 65.82; H, 4.64.

2,2-Difluoro6-(naft-2′-yl)-4-cinnamoyl-1,3,2-dioxaborine (**7a**). Dark orange powder, yield 11.0 %, melting point 242–243.3° c. ^{1}H NMR (400 MHz, $CDCl_3$), δ/ppm: 6.81 (s, 1H), 6.88 (d, *J* = 15.65 Hz, 1H), 7.4–7.52 (m, 3H), 7.58–7.71 (m, 4H), 7.89–8.06 (m, 4H), 8.14 (d, *J* = 15.65 Hz, 1H), 8.74 (s, 1H). ^{13}C NMR (101 MHz, $CDCl_3$), δ/ppm: 98.18, 120.67, 123.40, 127.39, 127.89, 129.00, 129.19, 129.24, 129.75, 129.98, 131.54, 131.95, 132.50, 133.90, 136.45, 147.78, 180.53, 182.27. IR (KBr), x/cm^{-1}: 3150 (OH_{ass}), 3061, 3024 (C-H_{Ph}), 1626 (C═C), 1597 (C═O), 1535 (C═C), 1387 (д B-O), 1145, 1132 (д B-F), 1053 (д B-O). Mass spectrum (ESI-), *m/z* (I, %): 347 [M−H] (100). Anal. calc. for $C_{21}H_{15}BF_2O_2$, %: C, 72.45; H, 4.34. Found, %: C 72.42; H 4.36.

2,2-Difluoro6-(9′*N*-fluorene-2′-yl)-4-cinnamoyl-1,3,2-dioxaborine (**8a**). Red powder, yield 71.27 %, melting point 257.4–258.6° C.^{1}H NMR (400 MHz, CDCl $_3$), δ/ppm: 3.99 (s, 2H), 6.72 (s, 1H), 6.84 (d, *J* = 15.65 Hz, 1H) 7.41–7.51 (m, 5H) 7.59–7.67 (m, 3H) 7.85–7.93 (m, 2H) 8.05–8.17 (m, 2H) 8.31 (s, 1H). ^{13}C NMR (101 MHz, $CDCl_3$), δ/ppm: 36.81, 97.80, 109.93, 120.22, 121.33, 125.39, 129.07, 129.19, 131.74, 134.01, 139.99, 143.83, 144.89, 147.11, 149.00, 179.76, 182.39. IR (KBr), υ/cm^{-1}: 3130 (OH_{ass}), 3065, 030 (C-H_{Ph}), 1626 (C═C), 1610 (C═O), 1537 (C═C), 1386, 1371 (δ B-O), 1197, 1180, 1153 (δ B-F), 1087, 1057 (δ B-O) Mass spectrum (ESI−), *m/z* (I, %):$[M + Na]^+$ 421 (100). Anal. calc. for $C_{24}H_{17}BF_2O_2$, %: C, 74.64; H, 4.44. Found, %: C 74.62; H 4.46.

2,2-Difluoro6-(1′-phenylphen-4′-yl)-4-cinnamoyl-1,3,2-dioxaborine (**9a**). Yellow powder, yield 65.5 %, melting point 243.6–244.5° C. ^{1}H NMR (400 MHz, $CDCl_3$), δ/ppm: 6.70 (s, 1H), 6.85 (d, *J* = 15.53 Hz, 1H), 7.48 (s, 6H), 7.66 (s, 4H), 7.77 (m, *J* = 8.56 Hz, 2H), 8.13 (d, *J* = 15.65 Hz, 1H), 8.18 (m, *J* = 8.56 Hz, 2H). ^{13}C NMR (101 MHz, $CDCl_3$), δ/ppm: 97.79, 120.65, 127.31, 127.65, 128.84, 129.08, 129.17, 129.23, 129.49, 131.93, 133.90, 147.68, 180.44, 182.01. IR (KBr), υ/cm^{-1}: 3136 (OH_{ass}), 3057, 3028 (C—H_{Ph}), 1637 (C═C), 1606 (C═O), 1568, 1542 (C═C), 1384 (δ B-O), 1143, 1126 (δ B-F), 1074, 1051 (δ B-O). (ESI-), *m/z* (I, %): 297 [M−C_6H_5] (50), 239 [M−C_6H_4−C_6H_5] (100). Anal. calc. for $C_{23}H_{17}BF_2O_2$, %: C, 73.83; H, 4.58. Found, %: C 73.78; H, 4.60.

2,2-Difluoro6-(*trans*-1′,2′-diphenylethylene-4′-yl)-4-cinnamoyl-1,3,2-dioxaborine (**10a**). Dark orange powder, yield 46.9 %, melting point 205.1–206.4° C. ^{1}H NMR (400 MHz, $CDCl_3$), δ/ppm: 6.66 (s, 1H), 6.83 (d, *J* = 15.65 Hz, 1H), 7.12–7.19 (m, 1H), 7.31 (d, *J* = 15.77 Hz, 2H), 7.36–7.49 (m, 5H), 7.56 (d, *J* = 7.46 Hz, 2H), 7.61–7.69 (m, 4H), 8.07–8.13 (m, 3H). ^{13}C NMR (101 MHz, $CDCl_3$), δ/ppm: 97.72, 120.70, 126.93, 127.01, 128.76, 128.86, 129.14, 129.21, 129.47, 130.41, 131.85, 133.05, 133.95, 136.30, 144.35, 147.41, 180.11, 181.57. IR (KBr), υ/cm^{-1}: 3126 (OH_{ass}), 3055, 3028 (C-H_{Ph}), 1631 (C═C), 1600 (C═O), 1539 (C═C), 1380 (δ B-O), 1184, 1126 (δ B-F), 1074, 1035 (δ B-O). (ESI−), *m/z* (I, %): 399 [M−H] (20). Anal. calc. $C_{25}H_{19}BF_2O_2$, %: C, 75.02; H, 4.70. Found, %: C 75.08; H, 4.69.

2.2. Measurements

Melting point was determined on a Buchi Melting Point B-540 instrument. IR spectra were recorded on a Spectrum BX 400 FTIR spectrometer (Perkin Elmer, USA) in potassium bromide. Mass spectra were recorded in the mode of registration of positive and negative ions, the ESI ionization source, the Shimadzu LCMS-2010EV mass spectrometric detector in the system acetonitrile:water – 9:1. NMR spectra were recorded using an Avance II 400 MHz high resolution spectrometer (Bruker, Germany) on ^{1}H and ^{13}C nuclei at various operating frequencies. Deuterated chloroform was used as a solvent. Absorption spectra were recorded on a Shimadzu UV 2550 spectrophotometer (Japan), Shimadzu UV 3101 PC (Japan). Luminescence and excitation spectra were obtained using a Shimadzu RF 5301 spectrofluorimeter (Japan) and PicoQuant FluoTime 200 fluorometer (Germany) A solution of anthracene in ethanol was used as a standard for measuring the fluorescence quantum yield (ϕ = 0.27) [40].

2.3. Calculations

Quantum chemistry simulation of electronic absorption spectra of 1a-10a was carried out using the GAMESS VERSION = 30 SEP 2021 (R2 Patch 1) software complex [41] and Firefly version 8.2.0, build number 10203. The results of the comparative analysis of the calculation results are given in the table. The results obtained using GAMESS (B3LYP) are the closest to the experiment. A comparative study of various electron density functionals of the GAMESS and Firefly/ software complexes for the 1a spectra was carried out. B3LYP showed better convergence with the experiment. The compounds structural parameters, energy characteristics, and electronic structure were determined at complete geometry optimization in the 6-311G(d, p) basis by the nonempirical method and the density functional theory (DFT) with the exchange–correlation potential B3LYP [42]. Electronic absorption spectra of compounds taking into account excited singlet states were calculated by the TDDFT method in the 6-311G(d, p) basis with the B3LYP potential. The effect of the solvent was taken into account using the PCM model for solvents (CCl_4, $CHCl_3$, $CH2Cl_2$, acetone). Visualization of the obtained data was carried out using the ChemCraft program,

2.4. Confocal microscope

HCT116 cells were grown in 35 mm dishes with a glass bottom until confluence of 50 % (SPL, Korea) in DMEM culture medium (10 % Fetal Bovine Serum). To determine intracellular localization of dyes **4a, 6a, 7a**, human colon carcinoma HCT116 cells were incubated with **4a, 6a, 7a** (5 μM) in culture medium (10 % DMEM) for 12 h, then washed with PBS. Compounds **4a, 6a, 7a** were detected in the range 450–550 nm, λ_{ex} = 405 nm in PBS. Laser scanning confocal microscope Leica TCS SPE 5 with LAS AF software (Leica Microsystems GmbH, Germany) was used for registration.

2.5. Cell culture

The human colon adenocarcinoma cell line HCT116 was obtained from the American Type Culture Collection (Manassas, VA). Cells were propagated in Dulbecco's modified Eagle's medium supplemented with

10 % fetal bovine serum (HyClone, Logan, UT), 2 mM L-glutamine, 100 U/mL penicillin and 100 μg/mL streptomycin (PanEco, Russia) at 37 °C, 5 % CO_2 in a humidified atmosphere. Cells in the logarithmic phase of growth were used in the experiments.

2.6. Cytotoxicity studies

The cytotoxic activity of compounds was assessed *in vitro* using the MTT assay against human colon cancer cells HCT116. Cells were plated in 96 well plates (NUNC, USA, $5{\cdot}10^3$ cells in 190 μl culture medium per well). After 24 h of incubation at 37 °C (5 % CO_2, in a humidified atmosphere), 10 μl cell media solutions of compounds (from 1 mM stocks in DMSO, stored a +4 °C, thawed at room temperature immediately before use) for final concentrations 0.9–15 μmol/L were added. Dark cytotoxicity of compounds was assessed in a formazan conversion assay (MTT-test) after a 72 h drug exposure. After the completion of drug exposure in the dark, 0.5 mg/ml 3-(4,5-dimethylthiazol-2-yl)-2,5-diphenyltetrazolium bromide (MTT reagent) was added to cells. Cells were incubated with MTT for 2 h, the culture medium was removed, the cells were re-suspended in 100 μl DMSO, and the optical density of the solution was measured on a Multiscan FC plate spectrophotometer (Thermo Scientific, USA) at a wavelength of 571 nm. The percentage of survived cells for each dose was calculated as the quotient of the average optical density in the wells after incubation with this dose to the average optical density of the control wells (the values of the latter are taken as 100 %). Four independent experiments were performed for each concentration. Standard deviations did not exceed 10 %.

3. Results and discussion

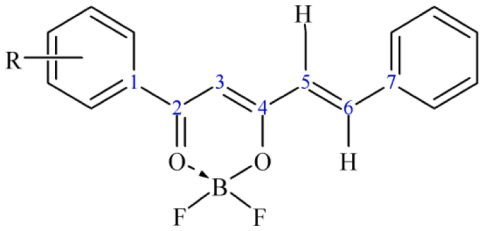
3.1. Synthesis of 1-arene-5-phenylpent-2,4-diene-1-onates of boron difluoride

In this work, we synthesized a number of 1-arene-5-phenylpent-2,4-diene-1-onates of boron difluoride **1a-10a** (Fig. 2) by aldol-croton condensation of benzaldehyde with arenoylacetonates of boron difluoride (**1**–**10**). The following conditions were selected: ethylacetate was used as a solvent and butylamine as a base, the yield of the resulting compounds was from 11 to 75 %.

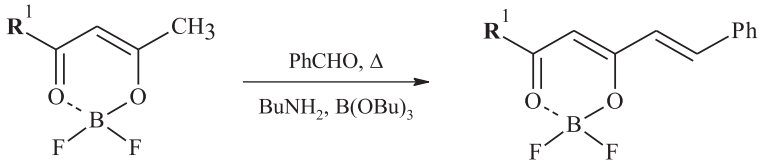
3.2. Electronic structure of compounds *1a-10a*

Optimization of geometry in the ground and excited state and modeling of absorption spectra were carried out for complexes **1a-10a.** For all complexes, the obtained regularities of changes in spectral properties in a series of compounds **1a-10a** in one solvent and one compound in a series of solvents are in good agreement with the experiment (ESI Tables 2S-6S). The structure of the boundary orbitals and the bond lengths of the molecule do not undergo significant changes during the transition from the vacuum approximation to taking into account the interaction with the solvent (PCM), this allows the discussion to use the results of calculations in the vacuum approximation. During vibrational relaxation in the excited state ($S_1 \rightarrow S'_1$) for the dyes **1a**–**4a**, there is observed a decrease of the length of single bonds between the chelate ring and the substituent, between the phenyl ring and the double bond. The Table 1 shows the bond lengths that undergo the greatest change during relaxation of the molecule in the excited state. The length of the C—C bonds of the chelate ring for **1a**–**4a** increases. At the same time, an increase of the length of double bonds is observed (Table 1). The length of the C1-C2 bond between the α-substituent and the chelate ring in the S'_1 geometry decreases for **1a-4a** and increases for **5a-10a.** The bond lengths of the C2-C3 and C3-C4 chelate cycle for **1a-5a** are aligned, and for **6a-10a** the C2-C3 bond is shortened, C3-C4 is lengthened (Table. 1). For all complexes in the S'_1 geometry, the

Table 1
Calculated lengths of C—C bonds (Å) in the studied complexes in the ground (**1a-10a**) and excited relaxed (**1a*-10a***) state in vacuum approximation.



	C1-C2	C2-C3	C3-C4	C4-C5	C5-C6	C6-C7
1a	1.477	1.396	1.400	1.452	1.349	1.459
1a*	1.448	1.420	1.417	1.270	1.383	1.455
2a	1.473	1.398	1.399	1.453	1.349	1.459
2a*	1.455	1.404	1.437	1.415	1.388	1.423
3a	1.473	1.398	1.398	1.453	1.349	1.458
3a*	1.456	1.402	1.439	1.414	1.389	1.427
4a	1.473	1.398	1.398	1.453	1.349	1.459
4a*	1.464	1.392	1.442	1.403	1.391	1.426
5a	1.477	1.400	1.399	1.453	1.349	1.458
5a*	1.505	1.346	1.456	1.393	1.391	1.432
6a	1.468	1.400	1.399	1.453	1.349	1.458
6a*	1.494	1.363	1.466	1.399	1.396	1.424
7a	1.474	1.397	1.399	1.451	1.349	1.458
7a*	1.507	1.349	1.453	1.397	1.390	1.433
8a	1.471	1.399	1.397	1.452	1.348	1.460
8a*	1.502	1.356	1.456	1.400	1.391	1.429
9a	1.473	1.397	1.399	1.452	1.349	1.459
9a*	1.425	1.369	1.449	1.402	1.387	1.431
10a	1.471	1.398	1.399	1.452	1.349	1.459
10a*	1.505	1.355	1.401	1.452	1.388	1.432



1-10 **1a-10a**

R^1 = Ph- (1a); R^1 = 4-CH_3-C_6H_4- (2a); R^1 = 4-Et-C_6H_4- (3a);

R^1 = 3,4-CH_3-C_6H_3- (4a); R^1 = 2,5-CH_3-C_6H_3- (5a); R^1 = 4-CH_3O-C_6H_4- (6a);

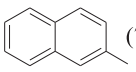
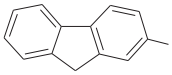
R^1 =  (7a); R^1=  (8a); R^1 = Ph-Ph- (9a); R^1 = Ph-CH=CH-Ph- (10a)

Fig. 2. Scheme of synthesis of the compounds **1a-10a.**

alignment of bond lengths and electron density for the fragment C4-C5=C6-C7 is observed: single bonds are shortened, and double bonds are lengthened, which contributes to the delocalization of the electron density in the S'_1 state. One should mention that, in the ground and excited states, alternating charges and bond orders are observed in the dye molecules (Table 1), which are similar to alternating charges in polymethine dyes. Therefore, for boron difluoride curcuminoids, changes in the geometry of molecules during relaxation in the excited state are similar to the changes occurring during the transition of polymethine dyes from neutral polyene to polymethine [43]. Here, the efficiency of the π-π conjugation in a molecule increases, and the transfer of electron density from the substituent to the stilbenyl fragment and the planarity of the substituent in the excited relaxed state increase, which contributes to the formation of a conjugative π-system of the molecule (Fig. 3).

All the complexes can be divided into two groups: 1) **1a-4a** with alkyl σ-donor substituents in the phenyl ring**,** for which the bond between the α-substituent and the chelate ring (C3-C4 and C4-C5) in the geometry S'_1 is shortened, the electron density on the HOMO is evenly distributed over the molecule, and on the LUMO is localized on the chelate cycle and double bond (Fig. 3); 2) **6a-10a**, in the geometry of the ground and excited relaxed states, the electron density is localized on the aromatic α-substituent and the chelate cycle, during the HOMO-LUMO transition, the electron density transferred from the α-substituent to the stilbenyl fragment (Fig. 3).

The electron density, in contrast to the geometry of S_0, is almost completely localized on the aromatic α-substituent. For the second group of compounds **6a-10a**, when the molecules are excited, the Intramolecular Charge Transfer (ICT) is realized. The structure of the frontiers orbitals **7a** in the geometry of the ground and excited relaxed states is shown (Fig. 4).

3.3. *Spectral properties of curcuminoids **1a-10a***

Absorption, excitation and luminescence spectra were recorded for the synthesized complexes. The absorption and excitation spectra of the complexes practically coincide for each of the compounds **1a-10a** (ESI Tables 2S-6S, Figs. 32S-35S). Curcuminoid **1a** was chosen as the standard to identify the effect of substituents on the luminescent properties of the prepared dyes, since this compound has no substituents in phenyl rings and is very simple in structure. When comparing the absorption and luminescence spectra (Fig. 5) of compounds he following regularities can be noted: when alkyl substituents (σ-donors) are introduced into the phenyl ring in the samples **1a-5a**, a slight bathochromic shift of the maxima of the luminescence spectra (5–7 nm) is observed (Figs. 5, 32S-35S).

For **1a-10a**, the structure of the absorption and luminescence spectra depends not only on the structure of the molecule, but also on the polarity of the solvent. In carbon tetrachloride, an almost nonpolar solvent, the spectra of all complexes have an vibronic structure, the absorption and luminescence spectra clearly show bands of 0–0 and 0–1 transitions (Figs. 5, 32S-35S). In a much more polar acetone, for most spectra, the vibrational structure disappears and one broad band is observed in the luminescence spectra. In other solvents, the spectra of **1a-5a** are structured, unlike the spectra of **6a-10a**. Such an effect for organic compounds is usually associated with a decrease in energy and convergence of energy levels under the action of the solvent field, while the vibrational sublevels merge [44].

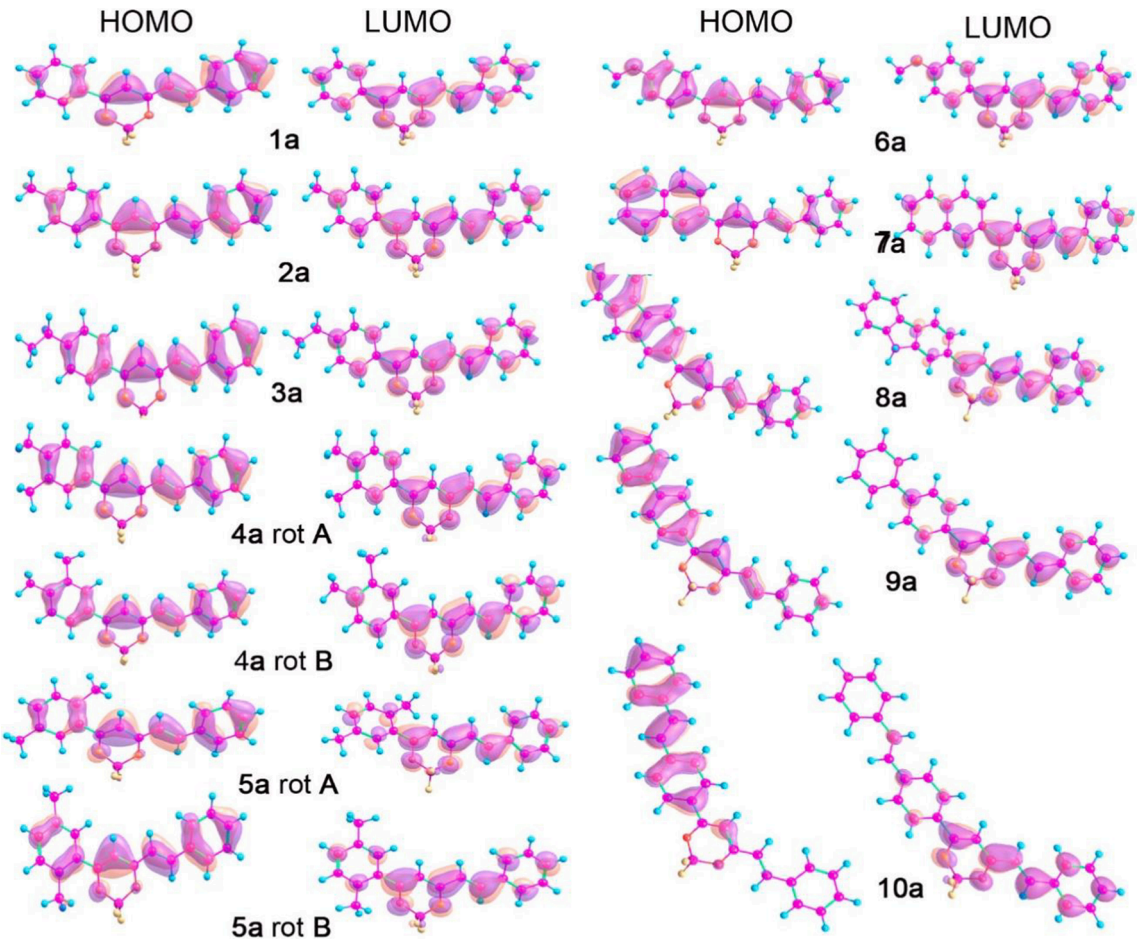


Fig. 3. Frontier molecular orbitals of the compounds **1a-10a**.

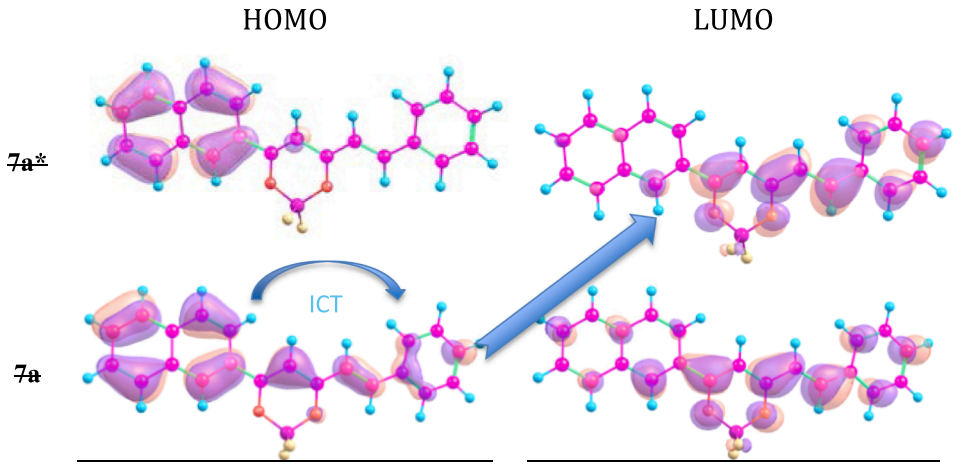


Fig. 4. ICT formation in molecule **7a** during photoexcitation.

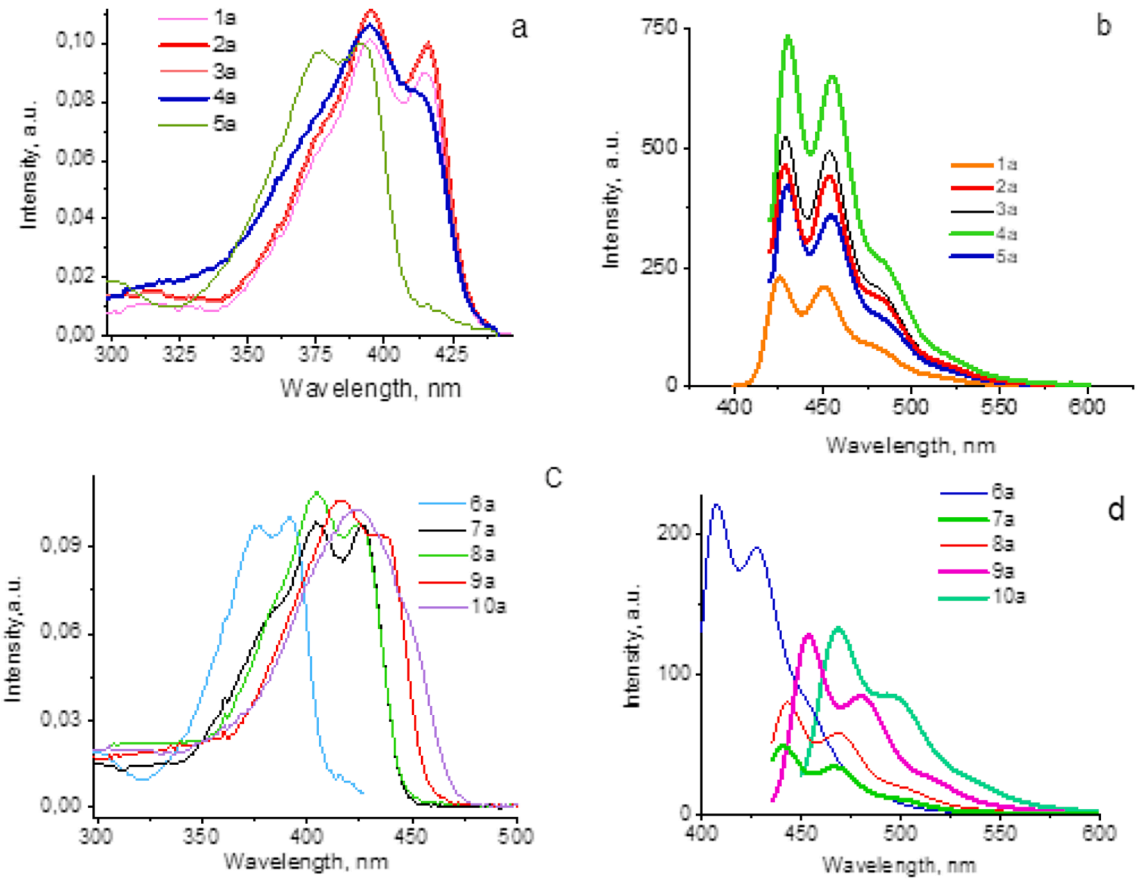


Fig. 5. Absorption (right) and luminescence (left) spectra **1a-10a** in tetrachlormethane.

The Stokes shift of **1a-4a** varies very slightly and equals to 23–24 nm. The quantum yield of luminescence **1a-5a** is 0.02–0.15 (Table 3). When introducing π-donor substituents such as the methoxy group **(6a)**, quantum yield increases to 0.87–0.95 and luminescence maxima shifts with increasing polarity from 409 to 440 nm. For curcuminoids with an extended π-system **(7a-10a)**, a bathochromic shift of the maxima of the absorption to 417–440 nm and luminescence spectra to 460–560 nm is observed (Figs. 5, 32S-35S). With an increase in the π-conjugation in the α-substituent, the quantum yield of luminescence increases in the following sequence: methoxyphenyl, naphthyl, diphenyl, fluorenyl, stilbenyl (Table 2). In a row 1a-10A with an increased of π-system the maxima of the absorption and luminescence spectra are significantly shifted to the red region as compared to **1a**, the quantum yield of luminescence for these compounds also increases (Tables 3, 2S-6S).

With an increase in the size of the molecule π-system in the series **1a-8a**, **10a**, the value of the Stokes shift increases markedly from 24 to 82 nm. In the series **1a-4a**, the position of alkyl groups in the phenyl substituent change, but the π-system of molecules remains virtually unchanged (Fig. 5), whereas the positions of the maxima of the absorption spectra and the value of the Stokes shift differ slightly (Table 4, Fig. 5). The introduction of the methoxy-group increases the π-system of the molecule by two π-electrons of the oxygen atom, while the maximum of

Table 2
Luminescence maximums of solutions and crystals of **1a-10a**.

N°	λ^*_{lum}, nm					λ_{lum}, nm crystals
	CCl_4	Dioxane	$CHCl_3$	CH_2Cl_2	Acetone	
1a	425, 452	435, 457	439, 460	445	444	536
2a	426, 453	432, 463	445, 468	449, 459	442, 457	523
3a	425, 453	437, 461	447, 461	445, 470	445, 461	544
4a	430. 455	440, 464	443, 460	445,472	445, 463	524
5a	431, 454	436, 462	442, 465	445	452	532
6a	409, 428	421	427	432	440	537
7a	442, 466	455, 462	460	490	505	544
8a	444, 470	454, 480	465	469	461	627
9a	454, 474	465	483	495	496	530
10a	470, 498	502	529	545	563	593

The maxima of 0–0 and 1–0 transitions are given for structured spectra.

Table 3
The quantum yield of luminescence (φ) of solutions of **1a-10a**.

N°	φ				
	CCl_4	Dioxane	$CHCl_3$	CH_2Cl_2	Acetone
1a	0.05	0.06	0.02	0.01	0,01
2a	0.12	0.10	0.09	0.08	0,07
3a	0.12	0.15	0.09	0.08	0,16
4a	0.15	0.14	0.11	0.13	0,32
5a	0.10	0.07	0.06	0.06	0,08
6a	0.87	0,98	0.95	0.95	0,95
7a	017	0,27	0.27	0.19	0,22
8a	0.30	0,19	0.20	0.21	0,23
9a	0.49	0,40	0.58	0.59	0,62
10a	0.57	0,57	0.50	0.52	0,21

Table 4
The Stokes shifts of solutions of **1a-10a**.

N°	$_{\Delta}\upsilon_{ST}$, cm^{-1}				
	CCl_4	Dioxane	$CHCl_3$	CH_2Cl_2	Acetone
1a	567	923	1113	1338	1458
2a	567	661	1438	1313	1766
3a	567	926	1236	1169	1281
4a	840	649	2692	1113	1394
5a	2373	2317	1770	2528	3129
6a	1191	1436	4665	1852	2462
7a	740	1551	1378	2423	3346
8a	2252	857	1568	1457	1456
9a	2117	547	4085	2371	2514
10a	2364	3833	4085	4357	4559

the absorption spectrum bathochromic shift. The replacement of the methoxy-group with phenyl leads to a further bathochromic shift of the maxima of the absorption spectra (Fig. 5b). The Stokes shift value increases along with the increase of the π-system: **1a** < **7a** < **9a** < **8a** < **10a** < **6a** (Table 4). At bathochromic the same time, the efficiency of electron density transfer from the phenyl substituent to the chelate cycle increases during the HOMO-LUMO transition (Fig. 3). Indeed, quantum chemical calculations show that, in the samples **1a, 6a**, **8a**, **10a (**phenyl, methoxyphenyl, fluorenyl, stilbenyl), the total energy of the molecule (E_{tot}) decreases: −1030.5, −1109.11, −1145.0, −1338.9 a.e. respectively, and the distance between the first and second energy levels decreases: ΔE = 3.60, 3.50, 3.45, 2.52 eV.

3.4. The effect of the steric factor on the luminescent properties of the complexes

The position of substituents in the phenyl ring has a significant effect on the luminescent properties of the obtained compounds, an illustrative example is the comparison of the luminescent properties of isomers **4a** and **5a** (Fig. 6). For these isomers, which differ only in the position of methyl groups in the phenyl α-substituent, the maxima of the spectra **5a** are hypsochromically shifted relatively to **4a**: luminescence by 3 nm, absorption (excitation) spectra by 10 nm (Fig. 6a, Table 2). For complex **5a**, an abnormally large value of the Stokes shift is observed in a number of compounds **1a-5a**: for **1a-4a**, 560–1300 cm^{-1}, depending on the polarity of the solvent, and for **5a** – 1700–3200 cm^{-1} (Table 3). This indicates another way of deactivating the excited state in **5a**.

According to the results of calculations for **5a**, there are two rotamers. In the **5a** molecule, the phenyl and chelate rings of **5a** cannot be located in the same plane due to the repulsion of the methyl group and the proton in the γ-position (rotamer **A**) or the methyl group and the oxygen atom of the chelate cycle (rotamer **B**) (Figs. 6c, 7). According to the calculation data, the angle between the planes of the phenyl substituent and the chelate cycle is 30° and, as a result, the π-π conjugation between the phenyl and β-diketonate cycles is weakening, and the electron density distribution on HOMO changes (Fig. 3). The conclusion about the non-planar structure of the **5a** molecule is consistent with the result of the analysis of the ^{1}H NMR spectra **4a** and **5a**, indicating a weak interaction of the phenyl substituent and the **5a** chelate cycle (ESI Figs. 4S,5S).

If for the rest of the studied complexes the bond length between the phenyl substituent and the chelate cycle decreases during the transition $S_1 \rightarrow S'_1$, in the case of **5a**, it increases to the value of the single bond (1.5 Å) (Table 2), the angle between the planes of the phenyl and chelate cycles also increases from 30 to 57°. The increase of the interplanar angle in the excited state is characteristic of the formation of Twisted Intramolecular Charge Transfer (TICT) [45,46]. The distribution of the electron density in the geometry of the excited relaxed state for **5a** is drastically different from the rest of the compounds: for **5a** HOMO, the electron density is completely concentrated on the phenyl substituent, for **1a-4a**, it is delocalized throughout the molecule (Fig. 8).

To sum up, for **5a** in S'_1 geometry, in contrast to the rest of the studied complexes, TICT is realized, which increases the Stokes shift and leads to the quenching of luminescence.

For a pair of compounds, **8a** and **9a**, which have the same number and location of π-electrons in the molecule, there is also a significant difference in spectral properties: the position of the maximum of the absorption spectrum differs by 32 nm, while that of luminescence – by 18 nm (Table 2, Fig. 9). The difference in the structure of the frontier orbitals **8a** and **9a** is much greater in the ground than in the excited relaxed state.

At comparing the initial compounds **8** and **9** (Fig. 2) with the same π-system of molecules, a difference in spectral properties was also revealed. For the initial compounds, **8** and **9**, the X-ray method established: 1) the planes of the first and second phenyl rings of molecule **9** are at an angle of 23.9° [39], the planes of the second phenyl and chelate rings are at an angle of 9.1°; for **9**, the dissipation of excitation energy by a non–radiative mechanism through the rotation of the phenyl rings is possible; 2) the methylene bridge between the phenyl rings in molecule

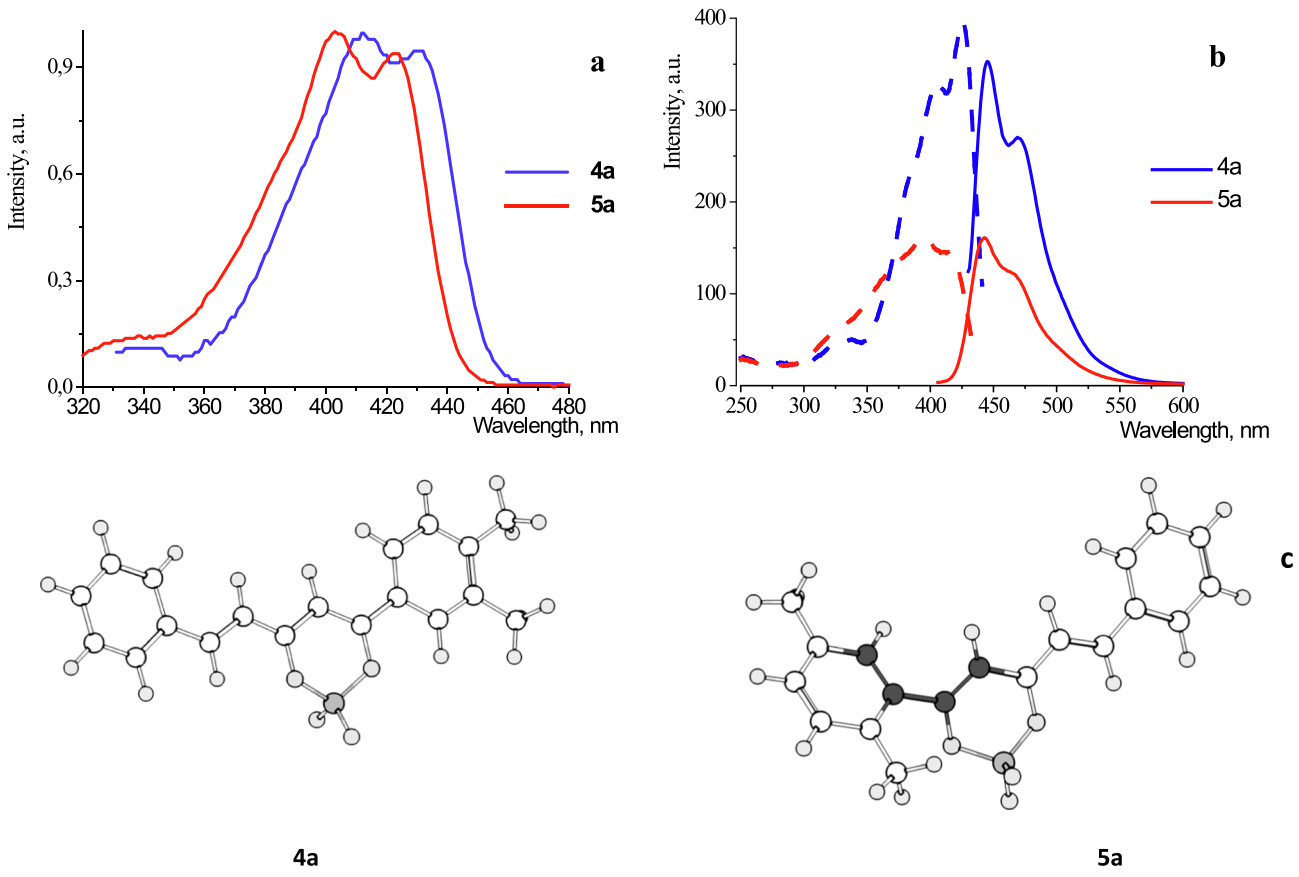


Fig. 6. (a) Absorption spectra of the solutions of **4a** and **5a** in chloroform, (b) excitation (dotted line) and luminescence (solid line) spectra of **4a** and **5a**, (c) optimized structures **4a** and **5a** in ground state.

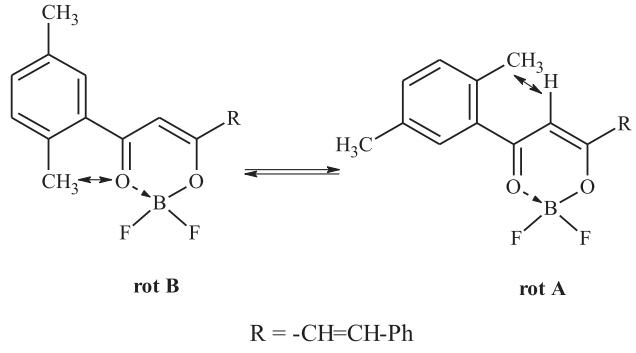


Fig. 7. Structure of rotamers **A** and **B** compound **5a**.

8 keeps them in the same plane and blocks the rotation of the second phenyl ring, which leads to increased conjugation in the molecule of **8**. Here, there is a bathochromic shift and a higher quantum yield of complex **8** compared to **9** [19].

A similar dependence is observed for **8a** and **9a;** the absorption and luminescence spectra of **8a** are bathochromically shifted relatively to the spectra of **9a** (Table 2), which could indicate a weakened conjugation in the dye molecule **9a** due to the removal of the second phenyl substituent from the plane of the molecule. Indeed, according to the calculation data, the angle between the planes of the diketonate cycle and the phenyl ring of the substituent for **9a** is 14°, while that between the planes of the diphenyl rings – 35°. In the **8a** molecule, the angle between the planes of the diketonate cycle and the substituent is 18°, while the substituent itself is flat (Fig. 9c). The strengthening of the coupling of the π-system in the **8a** molecule is also observed when comparing the bond lengths between the phenyl rings, **8a** (1.473 Å) and **9a** (1.483 Å). Thus, the structural features of 9a (the non-planar structure of the molecule) prevent the effective formation of excimers in crystals, leads to a decrease in the quantum yield and a noticeable hypsochromic shift in the luminescence spectra of solutions and crystals relative to 8a (Tables 2, 3).

3.5. *Spectral properties of crystals **1a-10a***

Fig. 10 shows photographs of solutions and crystals 1a-10a under UV light irradiation (365 nm). The luminescence color of solutions in a number of compounds varies from blue to yellow (420–560 nm). The prepared compounds **1a-10a** comprise crystalline substances with a color from yellow to red that exhibit a bright luminescence in the yellow-orange region (530–630 nm) (Table 2).

The excimer nature of the **1a-10a** luminescence is evidenced by the data of time-resolved luminescence spectroscopy (Fig. 11a,b, ESI Table 7S). The lifetime of **1a-10a** is in the range from 4 to 15 ns (ESI Table 7S), which is typical for excimers of boron difluoride β-diketonates [38,50]. The exception is **2a** with τ = 1.3 ns, in the series **1a-10a** (Fig. 11a,b, ESI Table 7S), for **2a** crystals the minimum half-width of the luminescence band is observed (Fig. 11c, ESI Fig. 36S).

The maximum of the luminescence and excitation spectrum of crystals is significantly shifted bathochromically relative to solutions (Table 2). In the excitation spectra of crystals, the long-wave band, assigns to the excitation of J-aggregates, prevails (Fig. 11). According to the X-ray data, β-diketonates of boron difluoride often form infinite stacks in crystals, representing J-aggregates consisting of H-dimers. In this case, the H-dimers act as an excimer traps and exhibit excimer luminescence [37–39].

For most β–diketonates of boron difluoride [51], such dimers consist

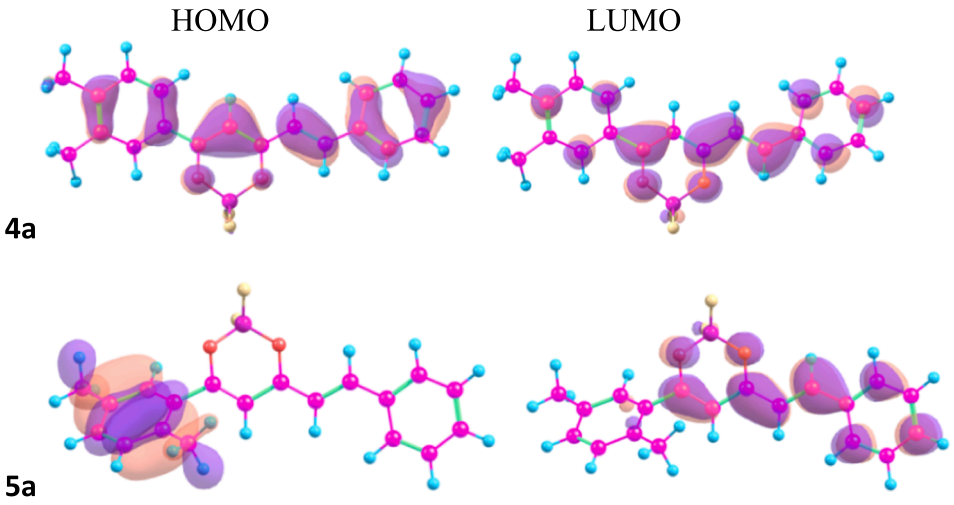


Fig. 8. Frontier orbitals of **4a** and **5a** in S'$_1$ geometry.

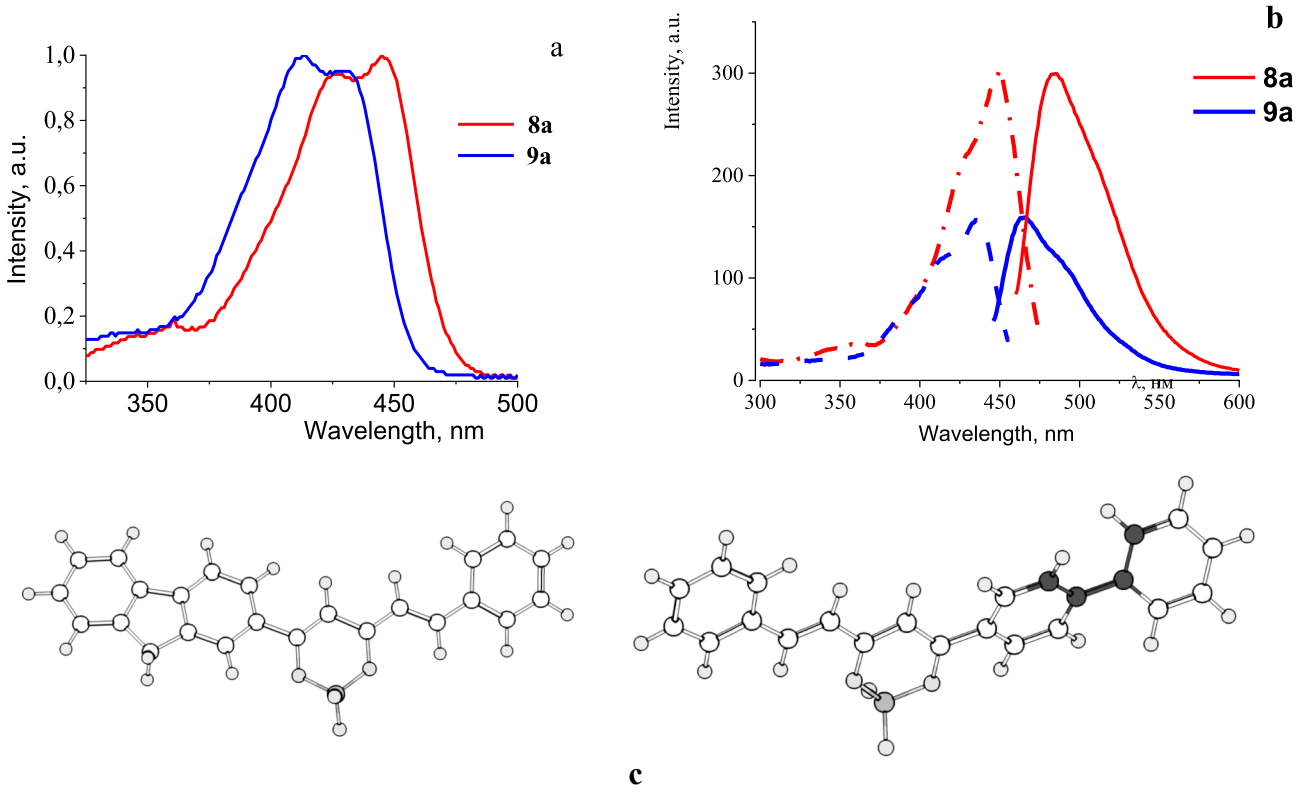


Fig. 9. (a) Absorption spectra of the solutions of compounds **8a** and **9a** in chloroform; (b) excitation (dotted line) and luminescence (solid line) spectra of the **8a** and **9a**, (c) optimized structure of **8a** (left) and **9a** (right) in ground state.

of antiparallel molecules in which the donor α–substituent of one molecule is located above the diketonate cycle of the neighboring one and vice versa. The structure of three complexes similar to the studied ones, boron difluoride 5-aryl-1-(2-hydroxyphenyl)pent-4-ene-1,3-dionates, is defined in [52], where the structure of dimers is shown. Based on the structural data [52] for the studied curcuminoids **1a** –**10a**, the structure of dimers forming excimers is proposed (Fig. 12).

The presence of fluorescence for aggregates and crystals of compounds **1a-10a** is a positive factor that allows them to be used for bio-visualization.

3.6. Bio-visualization

Fluorescent sensors combined with confocal microscopy imaging are a promising analytical tool for real-time monitoring of bio-endogenous molecules and environmental factors in living systems. Fluorescence spectroscopy is of broad interest in bioanalysis, especially in cell imaging, owing to its obvious advantages, such as sensitivity, speed, and the ability to perform real-time monitoring [47–49].

The dyes signals were registered in live HCT116 cells after 12 h of dye incubation using confocal microscopy. The compounds **4a, 6a, 7a** were not found in the nuclei. Compounds **4a, 6a, 7a** are diffusely distributed in the cytoplasm (Fig. 13).

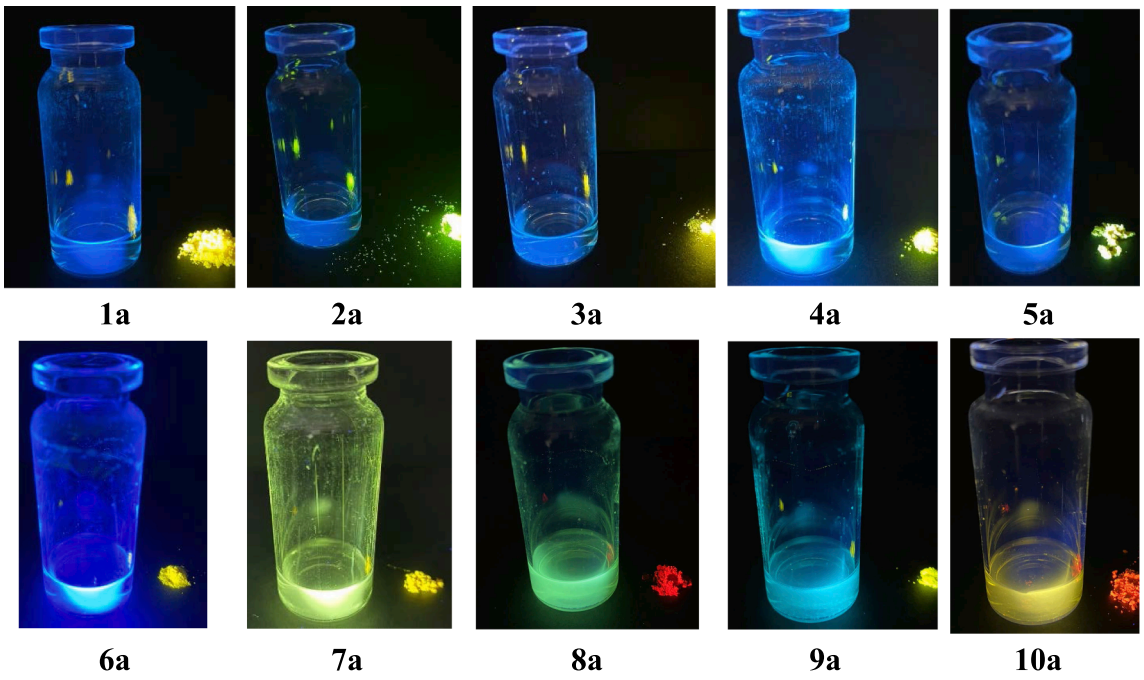


Fig. 10. Images of crystals and solutions in chloroform of the compounds **1a-10a** under UV irradiation (365 nm).

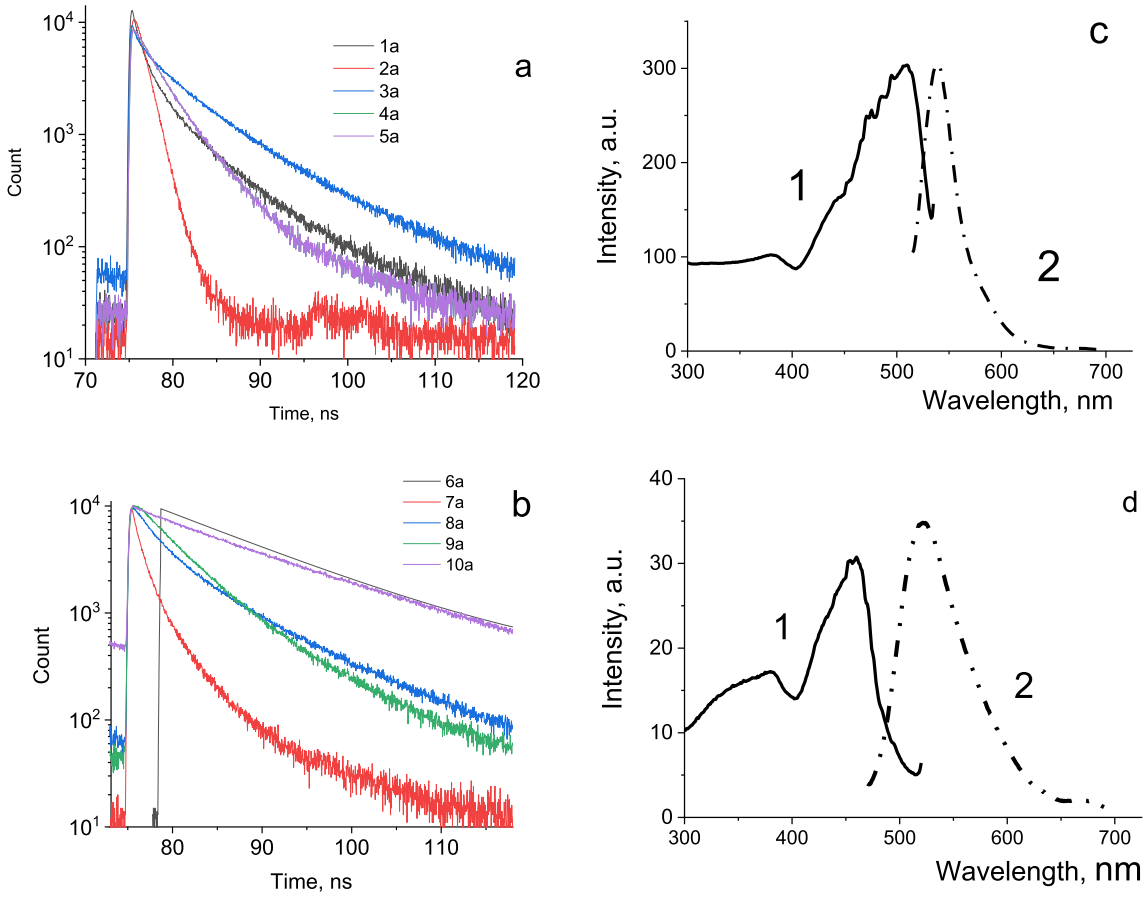


Fig. 11. (a) Kinetic curves of luminescence of crystals **1a-5a**; (b) kinetic curves of luminescence quenching of crystals **6a-10a**; (c) excitation (1) and luminescence (2) spectra of crystals **2**; (d) excitation (1) and luminescence (2) spectra of crystals **4a**.

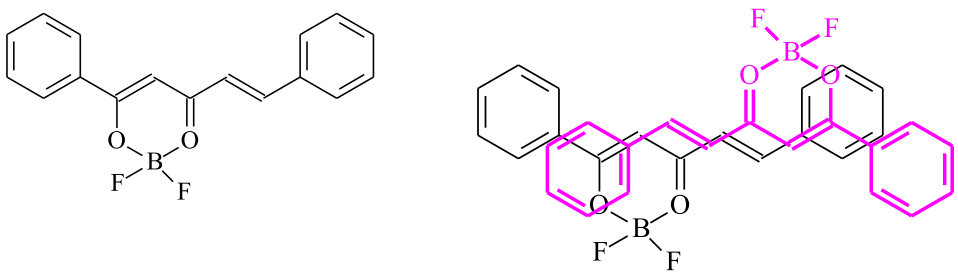


Fig. 12. (a) A base fragment of the structure of the curcuminoids studied in this work and in [52]; (b) the proposed structure of the **1a**-**10a** H-dimer.

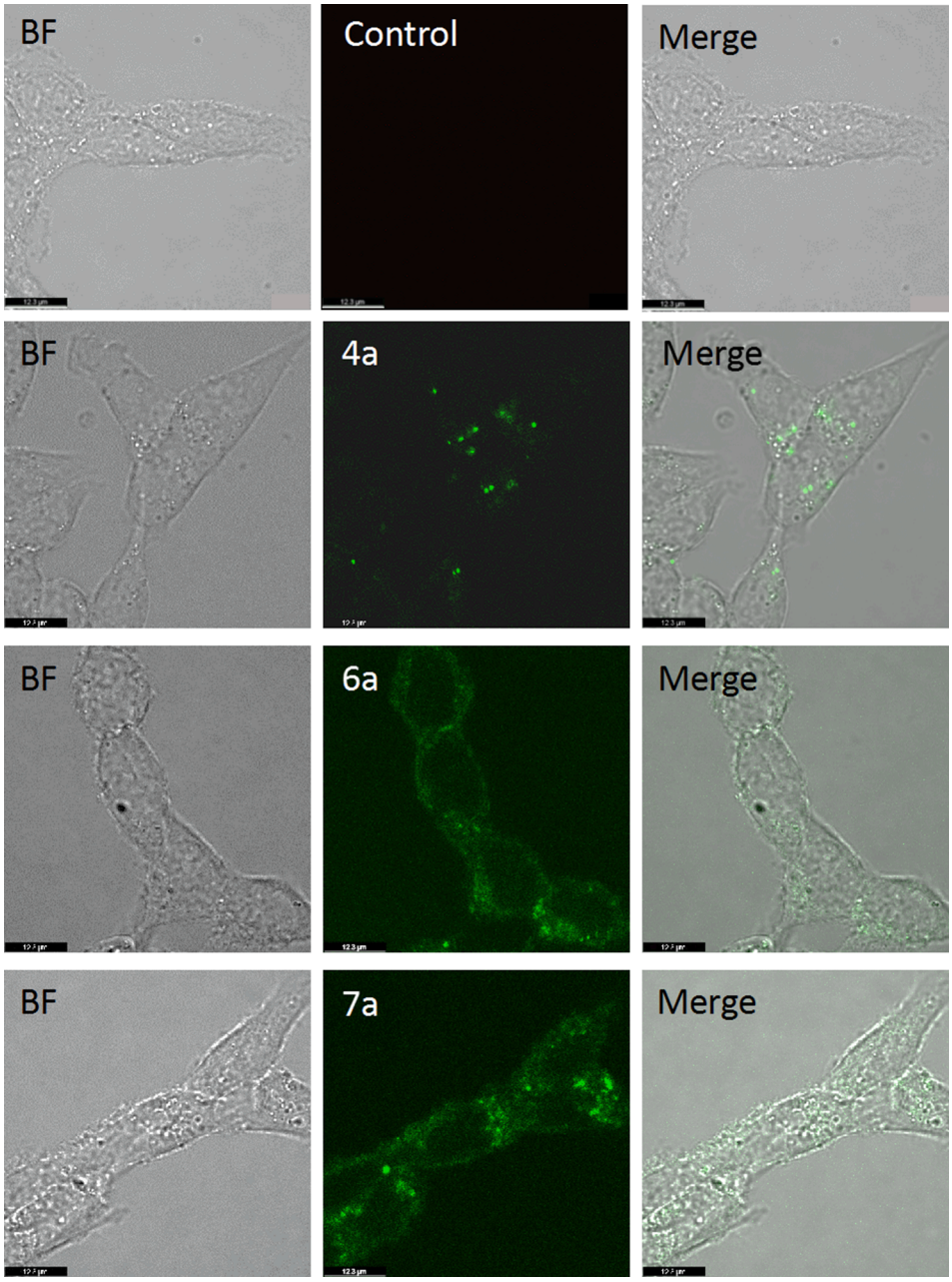


Fig. 13. Cytoplasmic distribution of compounds **4a**, **6a**, **7a** in HCT116 cells after 12 h incubation at final concentrations 5 μM (cells were washed with PBS after the incubation). Compounds were detected in the range 450–550 nm, $\lambda_{ex} = 405$ nm. Fields from left to right: bright field, fluorescence of the compound into the cell, image overlap.

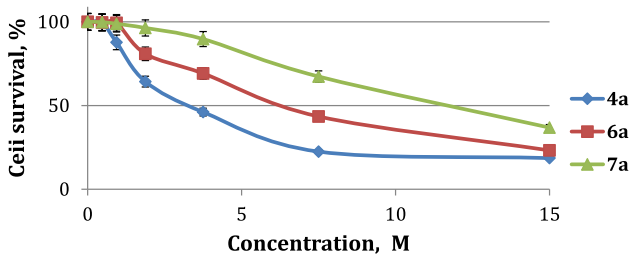


Fig. 14. Survival curves of HCT116 cells after 72 h incubation with **4a, 6a, 7a**.

Penetration of compounds into cells after 12 h of incubation does not disturb their morphology. Cells do not lose adhesion and do not have morphological signs of early death. Fluorescence of compounds **6a, 7a** is not too high; the signal is evenly distributed over the cytoplasm which allows you to visualize the entire cytoplasm of the cells. The fluorescent signal of compound **4a** is not uniformly distributed in a cell, which indicates selective accumulation in cell organelles. In accordance with the presence of fluorescence in the crystalline form of boron curcuminoids (Fig. 11), it can be assumed that the penetration of the studied compounds into the cell when introduced into the cell medium occurs in the form of aggregates that have their own fluorescence, which can be detected on a confocal microscope. This means that the synthesized boron curcuminoids do not require additional deaggregation during sample preparation for biovisualization. Although it is possible to assume an increase in their fluorescence due to spontaneous deaggregation by intracellular surfactants or proteins.

The dark cytotoxicity of boron curcuminoids on HCT116 human colon carcinoma cells was studied by the MTT test during long-term (72 h) incubation with cells (Fig. 14).

The data of the MTT test make it possible to determine the range of non-toxic concentrations of these compounds during long-term incubation with tumor cells. The compound **4a** demonstrated the most cytotoxic activity, with IC_{50} 3.1 ± 0.2 μM after 72 h incubation in the dark. Compounds **6a, 7a** had less cytotoxicity (up to 5 μM for 72 h) with IC_{50} values of 6.4 ± 0.4 and 11.7 ± 0.9 μM, respectively. The obtained curcuminoids of boron difluoride are promising for fluorescence imaging of cells at submicromolar concentrations at short incubation times and at less than 1 μM for long experiments, since cell death even after prolonged (72 h) incubation does not exceed 20 % of the control. Derivative **7a** is the lowest cytotoxic of the studied series, its concentrations for cell fluorescent visualization can be up to 5 μM.

We additionally studied the spectral characteristics of derivatives **4a**, **6a** and **7a** in water with different pH values. According to the pH range into the cell organelles from 4.5 (lysosomes) to 8.0 (nucleus) [53], we characterized the absorption and fluorescence of boron curcuminoids in this pH range. We also expanded the pH range to analyze the changes in the spectra under more severe conditions by adding measurements for pH 2 and 11. The data obtained are shown in Fig. 15 and in the supplementary materials in Figs. 37S, 38S.

The studied dependence of the spectral characteristics of **7a** at physiological pH values (4.5–7) there was no significant difference in both the absorption and the fluorescence intensity. However, for pH 8, which corresponds to a weak alkaline environment into the nuclei, a decrease in fluorescence was observed without significant change in absorption intensity at 405 nm. Also for a solution with a lowest pH 2, a bathochromic shift of the absorption spectrum was observed, and the absorption band at 450 nm became most pronounced. In the case of a highest pH 11, the opposite result was observed. At the extreme pH values, fluorescence was markedly reduced. Similar results were observed for compounds **4a** and **6a**, with the difference that in the neutral medium (pH 7) the fluorescence intensity was maxima for **4a** and its fluorescence in physiological pH range is less pH-dependent than for **6a** and **7a** with π-donor substituents. Thus, the absorbance spectra demonstrate that the compounds can be in two pH-dependent forms. In particular, for the compound **7a**, which has the best characteristics for biovisualization, the absorption band at 350–420 nm was more pronounced in an acidic medium, and 420–500 nm - in an alkaline medium.

Thus, the lead of synthesized boron curcuminoids **7a**, despite its weak fluorescence, have a number of interesting advantages for bioimaging: it can visualize acidic cell organelles (for example, lysosomes) and it also do not need to be disaggregated by surfactants after formation the aggregates or colloidal particles as a result of re-dissolution from DMSO into water, because they have its own fluorescence, sufficient to visualize the cytoplasm of cells. This means that for this series of compounds, when passing from spectral studies in cell-free systems to fluorescent staining of cells using these boron curcuminoids, it is possible not to carry out additional deaggregating sample preparation, and therefore, optimization (synthesis and bioimaging studies) of such structures for the tasks of enhancing fluorescence seems to be more simpler than in the case of popular hydrophobic fluorescent agents, which, when aggregated, lose fluorescence and require controlled disaggregation.

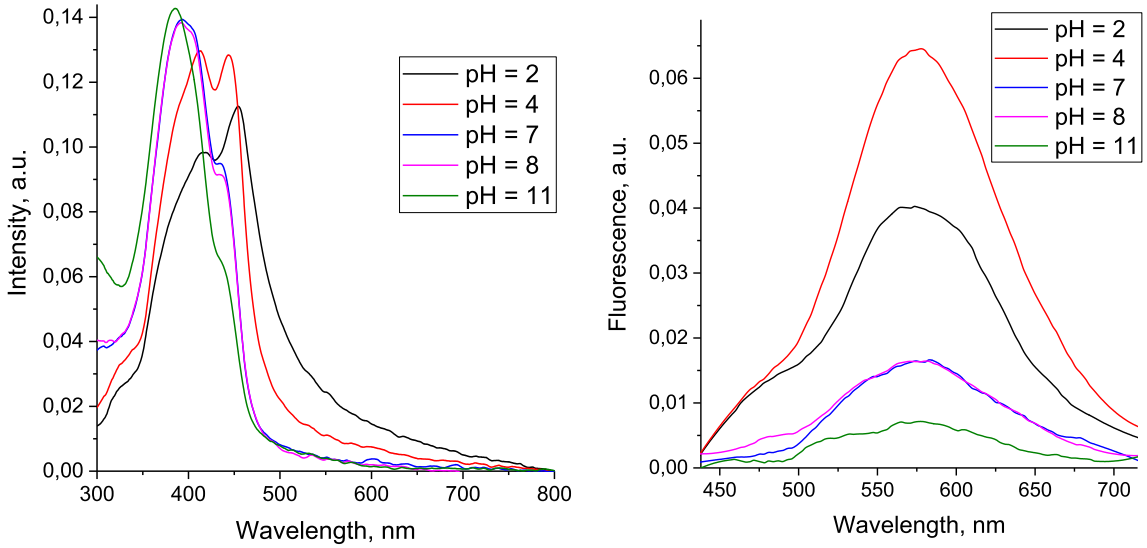


Fig. 15. Absorption (a) and fluorescence (b, λ_{exc} = 405 nm) spectra of **7a** in water solutions with different pH.

4. Conclusions

A comparative study of the electronic structure and luminescent properties of a series of boron difluoride curcuminoids: 1-aryl(getaryl)-5-phenylpent-2,4-diene-1-onates of boron difluoride (**1a-10a**) has been performed.

The influence of the electronic structure of α-substituents on the luminescence of the compounds has been revealed. The introduction of alkyl (σ-donor) substituents into the phenyl ring of chelates slightly increases the quantum yield and shifts the bathochromic luminescence spectra. In a series of complexes with alkyl substituents for **5a**, the presence of a methyl group in the *ortho*-position of the phenyl substituent, which prevents the flat structure of the molecule, contributes to the appearance of TICT, an increase in the Stokes shift, and a weakening of luminescence. Curcuminoids **6a-10a** with an extended π-system exhibit positive solvatochromism. The introduction of π-donor substituents leads to a noticeable bathochromic shift and an increase in the Stokes shift in the luminescence spectra. During the transition from σ-donor substituents in the phenyl ring to π-donor substituents, the quantum yield of luminescence increases from 0.03 to 0.22. The maximum Stokes shift and high quantum yield of luminescence are exhibited by the complex with a stilbene substituent, which has the longest π-system and the maximum charge transfer efficiency. The compounds **1a-10a** comprise crystalline substances with a color from yellow to red that exhibit a bright luminescence in the yellow-orange region (530–630 nm). The synthesized boron difluoride curcuminoids with a high luminescence quantum yield and a large Stokes shift are promising in terms of the development of luminescent smart materials.

The presented dyes are capable to penetrate into the cells of the model cell line and accumulate. The dyes **4a**, **6a**, **7a** accumulate mainly in the cytoplasm of cells. **6a** and **7a** are evenly distributed over the cytoplasm; the signal from **4a** indicates the selectivity of its accumulation. After 72 h of incubation these derivatives with cells, **4a** has the highest cytotoxicity, while **7a** has the lowest. Thus, compound **7a** is promising for visualization of the cell cytoplasm and acidic organelles.

CRediT authorship contribution statement

Anatolii G. Mirochnik: Supervision, Conceptualization, Methodology, Investigation, Writing – original draft, Resources, Writing – review & editing, Validation. **Zakhar N. Puzyrkov:** Investigation, Writing – original draft, Data curation. **Elena V. Fedorenko:** Project administration, Conceptualization, Methodology, Investigation, Data curation, Writing – original draft, Writing – review & editing. **Irina V. Svistunova:** Methodology, Investigation, Writing – original draft, Writing – review & editing, Validation. **Alina A. Markova:** Investigation, Writing – original draft. **Anna V. Shibaeva:** Investigation, Writing – original draft, Visualization. **Ivan D. Burtsev:** Investigation. **Alexey A. Kostyukov:** Investigation. **Anton E. Egorov:** Investigation. **Vladimir A. Kuzmin:** Conceptualization, Methodology, Investigation, Writing – original draft, Writing – review & editing.

Declaration of Competing Interest

The authors declare that they have no known competing financial interests or personal relationships that could have appeared to influence the work reported in this paper.

Data availability

No data was used for the research described in the article.

Acknowledgements

The work was supported by the Russian Science Foundation, project no.23-23-00461. Part of experiments cell studies and confocal microscopy experiments were performed in the Core Facility'New Materials and Technologies' at the N.M. Emanuel Institute of Biochemical Physics, Russian Academy of Sciences were supported by the Russian Federation State Program for this institution (Project №1202253303).

Appendix A. Supplementary data

Supplementary data to this article can be found online at https://doi.org/10.1016/j.saa.2023.122319.

References

[1] Y. Hong, J.W.Y. Lam, B.Z. Tang, Aggregation-induced emission, Chem. Soc. Rev. 40 (11) (2011) 5361.
[2] I.D.W. Samuel, G.A. Turnbull, Organic semiconductor lasers, Chem. Rev. 107 (2007) 1272–1295, https://doi.org/10.1021/cr050152i.
[3] C. Löwe, C. Weder, Oligo(p-phenylene vinylene) excimers as molecular probes: deformation-induced color changes in photoluminescent polymer blends, Adv. Mater. 22 (2002) 1625–1629, https://doi.org/10.1002/1521-4095(20021118)14:22<1625::AID-ADMA1625>3.0.CO;2-Q.
[4] F. Würthner, T.E. Kaiser, C.R. Saha-Möller, J-aggregates: from serendipitous discovery to supramolecular engineering of functional dye materials, Angew. Chem., Int. Ed. 50 (2011) 3376–3410, https://doi.org/10.1002/anie.201002307.
[5] T. Mutai, H. Satou, K. Araki, Reproducible on-off switching of solid-state luminescence by controlling molecular packing through heat-mode interconversion, Nat. Mater. 4 (2005) 685–687, https://doi.org/10.1038/nmat1454.
[6] A.C. Grimsdale, K.L. Chan, R.E. Martin, P.G. Jokisz, A.B. Holmes, Synthesis of light-emitting conjugated polymers for applications in electroluminescent devices, Chem. Rev. 109 (2009) 897–1091, https://doi.org/10.1016/j.jlumin.2021.118043.
[7] S. Bou, A.S. Klymchenko, M. Collot, Fluorescent labeling of biocompatible block copolymers: synthetic strategies and applications in bioimaging, Mater. Adv. 2 (2021) 3213–3233, https://doi.org/10.1039/d1ma00110h.
[8] M. Elbing, G.C. Bazan, A new design strategy for organic optoelectronic materials by lateral boryl substitution. Angew. Chem. Int. Ed. Engl. 47 (2008) 834−838, https://doi.org/10.1002/anie.200703722.
[9] G.M. Farinola, R. Ragni, Electroluminescent materials for white organic light emitting diodes, Chem. Soc. Rev. 40 (2011) 3467–3482, https://doi.org/10.1039/c0cs00204f.
[10] Z. Shen, Y. Gao, M. Li, Y. Zhang, K. Xu, S. Gong, Z. Wang, S. Wang, Development and application of a novel β-diketone difluoroboron-derivatized fluorescent probe for sensitively detecting H_2S, Spectrochim. Acta A 281 (2022), 121609, https://doi.org/10.1016/j.saa.2022.121609.
[11] M. Irie, T. Fukaminato, T. Sasaki, N. Tamai, T. Kawai, A digital fluorescent molecular photoswitch, Nature 420 (2002) 759–760, https://doi.org/10.1038/420759a.
[12] B. Vedhanarayanan, V.K. Praveen, G. Das, A. Ajayaghosh, Hybrid materials of 1D and 2D carbon allotropes and synthetic π-systems, NPG Asia Mater. 10 (2018) 107–126, https://doi.org/10.1038/s41427-018-0017-6.
[13] S. Ghosh, S. Cherumukkil, C.H. Suresh, A. Ajayaghosh, Supramolecular nanocomposite as near infrared transmitting optical filter for security and forensic applications, ACS Adv. Mater. 29 (2017) 1703783, https://doi.org/10.1002/adma.201703783.
[14] S.-J. Yoon, J.W. Chung, J. Gierschner, K.S. Kim, M.-G. Choi, D. Kim, S.Y. Park, Multistimuli two-color luminescence switching via different slip-stacking of highly fluorescent molecular sheets, J. Am. Chem. Soc. 132 (39) (2010) 13675–13683.
[15] Z. Chi, X. Zhang, B. Xu, X. Zhou, C. Ma, Y. Zhang, S. Liu, J. Xu, Recent advances in organic mechanofluorochromic materials, Chem. Soc. Rev. 41 (2012) 3878–3896, https://doi.org/10.1039/C2CS35016E.
[16] J. Guo, C. Zhou, S. Xie, S. Luo, T.Y. Gopalakrishna, Z. Sun, J. Jouha, J. Wu, Z. Zeng, Large aromatic hydrocarbon radical cation with global aromaticity and state-associated magnetic activity, Chem. Mater. 32 (2020) 5927–5936, https://doi.org/10.1021/acs.chemmater.9b05099.
[17] X. Deng, X. Liu, L. Wei, T. Ye, X. Yu, C. Zhang, J. Xiao, Pentagon-containing π-expanded systems: synthesis and photophysical properties, J. Org. Chem. 86 (15) (2021) 9961–9969.
[18] B.M. Krasovitskii, B.M. Bolotin, Organic Luminescent Materials. Weinheim, 1988. 340 pp.
[19] B.V. Bukvetskii, E.V. Fedorenko, A.G. Mirochnik, Crystal structure and luminiscent properties of 2,2-difluoro-4-(9h- fluorene-2-yl)-6-methyl-1,3,2-dioxaborine, J. Struct. Chem. 52 (2011) 221–225, https://doi.org/10.1134/S0022476611010331.
[20] A. Wakamiya, K. Mori, S. Yamaguchi, 3-Boryl-2,2'-bithiophene as a versatile core skeleton for full-color highly emissive organic solids, Angew. Chem., Int. Ed. 46 (2007) 4273–4276, https://doi.org/10.1002/anie.200604935.
[21] P.-Z. Chen, L.-Y. Niu, Y.-Z. Chen, Q.-Z. Yang, Difluoroboron β-diketonate dyes: Spectroscopic properties and applications, Coord. Chem. Rev. 350 (2017) 196–216, https://doi.org/10.1016/j.ccr.2017.06.026.
[22] A.G. Mirochnik, B.V. Bukvetskii, E.V. Gukhman, V.E. Karasev, Crystal structure and excimer fluorescence of some benzoylacetonatoboron difluorides: stacking factor, J. Fluoresc. 13 (2003) 157–162, https://doi.org/10.1023/A:1022939209971.

[23] A. D'Aléo, A. Felouat, V. Heresanu, A. Ranguis, D. Chaudanson, A. Karapetyan, M. Giorgi, F. Fages, Two-photon excited fluorescence of BF2 complexes ofcurcumin analogues: toward NIR-to-NIR fluorescent organic nanoparticles, J. Mater. Chem. 2 (26) (2014) 5208–5215.
[24] G. Zhang, J. Lu, M. Sabat, C.L. Fraser, Polymorphism and reversible mechanochromic luminescence for solid-state difluoroboron avobenzone, J. Am. Chem. Soc. 132 (2010) 2160–2162, https://doi.org/10.1021/ja9097719.
[25] M. Liu, L. Zhai, J. Sun, P. Xue, P. Gong, Z. Zhang, J. Sun, R. Lu, Multi-color solidstate luminescence of difluoroboron β-diketonate complexes bearing carbazole with mechanofluorochromism and thermofluorochromism, Dyes Pigm. 128 (2016) 271–278, https://doi.org/10.1016/j.dyepig.2016.02.005.
[26] M. Louis, C. Piñero García, A. Brosseau, C. Allain, R. Métivier, Mechanofluorochromism of a difluoroboron-β-diketonate derivative at the nanoscale, J. Phys. Chem. Lett. 10 (16) (2019) 4758–4762.
[27] Y.Q. Dong, J.W.Y. Lam, B.Z. Tang, Mechanochromic luminescence of aggregation-induced emission luminogens, J. Phys. Chem. Lett. 6 (2015) 3429–3436, https://doi.org/10.1021/acs.jpclett.5b01090.
[28] M.R. Hayes, J. Metcalfe, The boron-curcumin complex in the determination of trace amounts of boron, Analyst 87 (1962) 956–969, https://doi.org/10.1039/AN9628700956.
[29] C. Ran, X. Xu, S.B. Raymond, B.J. Ferrara, K. Neal, B.J. Bacskai, Z. Medarova, A. Moore, Design, synthesis, and testing of difluoroboron-derivatized curcumins as near-infrared probes for in vivo detection of amyloid-β deposits, J. Am. Chem. Soc. 131 (2009) 15257–15261, https://doi.org/10.1021/ja9047043.
[30] Z. Sui, R. Salto, J. Li, C. Craik, P.R.O. de Montellano, Inhibition of the HIV-1 and HIV-2 proteases by curcumin and curcumin boron complexes, Bioorg. Med. Chem. 1 (1993) 415–422, https://doi.org/10.1016/S0968-0896(00)82152-5.
[31] H. Tong, K. Lou, W. Wang, Near-infrared fluorescent probes for imaging of amyloid plaques in Alzheimer's disease. Acta Pharm. Sin. B, 7 (2015) 5–33, https://doi.org/10.1016/j.apsb.2014.12.00632.
[32] A.J. Yoon, H. Wu, R.D. Pan, B. Teter J. Cipolla, E. Chang, I.Z. Avila, S.K. Basak, E.S. Srivatsan, M. B. Wang, G.M. Cole, S.A. Frautschy, P.D. Hampton, K.F. Faull, LC-MS assay using derivatization with boron trifluoride to quantify curcuminoids in biological samples. Anal. Biochem. 596 (2020) 113636. https://doi.org/10.1016/j.ab.2020.113636.
[33] A. Gerasov, M. Shandura, Y.u. Kovtun, M. Losytskyy, V. Negrutska, I. Dubey, Fluorescent labeling of proteins with amine-specific 1,3,2-(2 H)-dioxaborine polymethine dye, Anal. Biochem. 420 (2012) 115–120, https://doi.org/10.1016/j.ab.2011.09.018.
[34] D. Delgado, R. Abonia, Synthetic approaches for BF2-containing adducts of outstanding biological potential. A review, Arab. J. Chem. 15 (1) (2022) 103528.
[35] A. Weissberger, E.S. Proskauer, J.A. Riddick, E.E. Toops, Organic Solvents. Physical Properties and Methods of Purification, Interscience Publ, New York, 1955, p. 552..
[36] V.E. Karasev, O.A. Korotkikh, Spectral-luminescence properties of F_2B - β–diketonates, Russ. J. Inorg. Chem. 31 (1986) 869–872.
[37] G. Görlitz, H. Hartmann, B. Nuber, A simple route to 4-aryl and 4-hetaryl substituted 6-methyl-2,2-difluoro-1,3,2-(2H)-dioxaborines, J. Prakt. Chem. 341 (1999) 167–172, https://doi.org/10.1002/chin.199922172.
[38] E.V. Fedorenko, A.G. Mirochnik, A.V. Gerasimenko, A.Y. Beloliptsev, Z. N. Puzyrkov, I.V. Svistunova, A.A. Sergeev, Fluorescence and phosphorescence of α- and β-isomers of boron difluoride naphthaloylacetonates, J. Photochem. Photobiol. A 412 (2021), 113220, https://doi.org/10.1016/j.jphotochem.2021.113220.
[39] B. V. Bukvetskii, E. V. Fedorenko, A. G. Mirochnik Crystal structure and luminescence of 2,2-difluoro-4-(4′-phenylphenyl)-6-methyl-1,3,2-dioxaborin ($C_6H_5C_6H_4COCHCOCH_3BF_2$). J. Struct. Chem., 51 (2010) 785–789, https://doi.org/:10.1134/10.1007/s10947-010-0118-8.
[40] A.M. Brouwer, Standards for photoluminescence quantum yield measurements in solution (IUPAC Technical Report), Pure Appl. Chem 83 (2011) 2213–2228, https://doi.org/10.1351/PAC-REP-10-09-31.
[41] M.W. Schmidt, K.K. Baldridge, J.A. Boatz, S.T. Elbert, M.S. Gordon, J.H. Jensen, S. Koseki, N. Matsunaga, K.A. Nguyen, S.J. Su, T.L. Windus, M. Dupius, J. A. Montgomery, General atomic and molecular electronic-structure system, J. Comp. Chem. 14 (1993) 1347–1363, https://doi.org/10.1002/jcc.540141112.
[42] A.D. Becke, Density-functional thermochemistry. III. The role of exact ex-change, J. Chem. Phys. 98 (1993) 5648–5652, https://doi.org/10.1063/1.464913.
[43] A.I. Tolmachev, A.Ya. Il'chenko. Polymethine dyes, in: Kirk-Othmer Encyclopedia of Chemical Technology. Hoboken, US: John Wiley and Sons, 20 (2005). 504-522.
[44] C. Reichardt, Solvents and Solvent Effects in Organic Chemistry, 2th Ed., Wiley-VCH, Weinheim, 2010, p. 718 S.
[45] S. Jana, S. Dalapati, S. Ghosh, N. Guchhait, Excited state intramolecular charge transfer process in 5-(4-dimethylamino-phenyl)-penta-2,4-dienoic acid ethyl ester and effect of acceptor functional groups, J. Photochem. Photobiol. A 261 (2013) 31–40, https://doi.org/10.1016/J.JPHOTOCHEM.2013.04.005.
[46] I. Georgieva, A.J.A. Aquino, S. Sasaki, G.P.C. Drummen, G. Konishiac, Recent advances in twisted intramolecular charge transfer (TICT) fluorescence and related phenomena in materials chemistry, J. Mater. Chem. C 4 (2016) 2731–2743, https://doi.org/10.1063/1.3270165.
[47] U. Schobel, H.J. Egelhaaf, A. Brecht, D. Oelkrug, G. Gauglitz, New donor-acceptor pair for fluorescent immunoassays by energy transfer, Bioconjug. Chem. 10 (1999) 1107–1114, https://doi.org/10.1021/bc990073b.
[48] D. Singharoy, S. Chowdhury, S.S. Mati, S. Ghosh, K. Chattopadhyay, S. C. Bhattacharya, Photoinduced electron transfer switching mechanism of a naphthalimide derivative with its solvatochromic behaviour: an experimental and Theoretical, Int. J. Hydrogen Energy 65 (2017) 16516–16524, https://doi.org/10.1002/chem.201702414.
[49] Y. Gao, M. Li, X. Tian, K. Xu, S. Gong, Y. Zhang, Y. Yang, Z. Wang, S. Wang, Colorimetric and turn-on fluorescent chemosensor with large stokes shift for sensitively probing cyanide anion in real samples and living systems, Spectrochim. Acta A 271 (2022), 120882, https://doi.org/10.1016/j.saa.2022.120882.
[50] B.V. Bukvetskii, E.V. Fedorenko, A.G. Mirochnik, Crystal structure and luminescence properties of 4-(4-benzoyloxy-2-hydroxyphenyl)-2,2-difluoro-6-phenyl-1,3,2-dioxaborine, Russ. Chem. Bull. 62 (9) (2013) 1991–1998.
[51] E.V. Fedorenko, A.G. Mirochnik, A.Y. Beloliptsev, Molecular design and luminescence of boron difluoride benzoylacetonates, J. Lumin. 196 (2018) 316–325, https://doi.org/10.1016/j.jlumin.2017.12.071.
[52] S. Guieu, J. Pinto, V.L.M. Silva, J. Rocha, A.M.S. Silva Synthesis, Post-modification and fluorescence properties of boron diketonate complexes, Eur. J. Org. Chem. 16 (2015) 423–3426, https://doi.org/10.1002/ejoc.201500318.
[53] A. Asokan, M.J. Cho, Exploitation of intracellular pH gradients in the cellular delivery of macromolecules, J. Pharm. Sci. 91 (2002) 903–913, https://doi.org/10.1002/jps.10095.